

Lorenz-like systems and classical dynamical equations with memory forcing: a new point of view for singling out the origin of chaos

R. Festa¹, A. Mazzino^{2,1} and D. Vincenzi^{3,1}

¹ *INFM–Department of Physics, University of Genova, I-16146 Genova, Italy*

² *CNR–ISIAAtA, Polo Scientifico dell’Università, I-73100 Lecce, Italy*

³ *CNRS, Observatoire de la Côte d’Azur, B.P. 4229, 06304 Nice Cedex 4, France*

(November 15, 2018)

Abstract

A novel view for the emergence of chaos in Lorenz-like systems is presented. For such purpose, the Lorenz problem is reformulated in a classical mechanical form and it turns out to be equivalent to the problem of a damped and forced one dimensional motion of a particle in a two-well potential, with a forcing term depending on the “memory” of the particle past motion. The dynamics of the original Lorenz system in the new particle phase space can then be rewritten in terms of an one-dimensional first-exit-time problem. The emergence of chaos turns out to be due to the discontinuous solutions of the transcendental equation ruling the time for the particle to cross the intermediate potential wall. The whole problem is tackled analytically deriving a piecewise linearized Lorenz-like system which preserves all the essential properties of the original model.

PACS number: 05.45.-a

I. INTRODUCTION

The Lorenz dynamical system, originally introduced by Lorenz [1] in order to describe in a very simplified way the Rayleigh-Bénard problem [2,3], immediately became important in itself as one of the most studied low-dimensional chaotic systems. Still today the Lorenz model represents a paradigmatic example for both theoretical and numerical investigations in checking some results in chaos theory [4–7], in the study of geometrical properties of dynamical systems [8–11], in nonlinear analysis of time series [12,13], in the stabilization and synchronization of coupled systems [14–16], and so on.

Nevertheless, despite the great attention attracted over past decades, some fundamental and rigorous results have been obtained quite recently, as for instance the proof of the existence of the Lorenz attractor [17,18], usually using somewhat sophisticated mathematical tools.

On the contrary, our aim here is to provide a description of Lorenz system dynamical features, which requires quite simple analytical tools and, at the same time, allows a very intuitive inspection in Lorenz-like chaos. Preliminary results have been reported in a short communication [19]. Here we shall give more details and new results.

Our interpretation will base itself upon the fact that in the “steady state”, i.e., far from the initial transient and when the memory of the initial conditions has been lost, the Lorenz system is equivalent to a suitably constructed second order integral-differential equation. This equation can be regarded, for instance, as a customary second order one-dimensional classical mechanics equation with a peculiar forcing term. The corresponding dynamics can be interpreted as the one-dimensional motion of a particle in a conservative quartic two-well potential, subjected to a viscous damping and to an additional force resulting from the past history of the motion. The latter force turns out to be essential for chaos to emerge as it acts as an “endogenous” forcing able to permanently sustain the motion even in presence of friction.

The previous interpretation of Lorenz dynamics actually leads to a generalization of the Lorenz model to a wider class of systems showing similar dynamical properties. We shall introduce a particular system belonging to such class which, because of its simplicity (piecewise linearity), will allow us to study the dynamics of the original model using analytical tools. Indeed, in the steady chaotic regime (i.e. when the system permanently lies on its attractor set) the evolution of a point in the Lorenz phase-space can be roughly described as a somewhat regular amplified oscillation around one of its fixed points, followed by a sudden entry in the control basin of a twin fixed point symmetrical with respect to the origin, by a new amplified oscillation around the latter point, by a sudden return in the control domain of the former, and so on.

The most evident aspect of the chaotic regime is just the unpredictability of the instant at which the center of the aforementioned amplified oscillations changes. The choice of a piecewise linearized version of the original model will allow us to highlight this point, while keeping unchanged the peculiar topological properties of the Lorenz dynamics. The exact equation ruling the instant of change of the oscillation center will be derived and a discontinuous dependence of this instant on the initial conditions will be highlighted. It will also be possible to write the analytical equations that defines the first-return two-dimensional Poincaré map for the piecewise linearized system, which in turn synthesizes the main chaotic features of the model dynamics. Moreover, we shall show that, under suitable and reason-

able conditions, the evolution of the system completely reduces to a one-dimensional chaotic map.

To summarize, starting from our interpretation, we shall be able to propose a piecewise linearized version of the Lorenz model, which on one hand has the same dynamical properties of the original system and, on the other hand, will provide analytical tools to explicate the emergence of chaos in Lorenz-like systems.

II. THE LORENZ EQUATION

The original Lorenz system [1] consists of the three first order ordinary differential equations

$$\begin{cases} \dot{X} = -\sigma X + \sigma Y \\ \dot{Y} = -Y + (r - Z)X \\ \dot{Z} = -bZ + XY, \end{cases} \quad (1)$$

where the dots indicate time derivatives and σ , b and r are positive parameters originally related to the fluid properties and to the boundary conditions in the Rayleigh-Bénard problem. (Lorenz [1] used $\sigma = 10$, $b = 8/3$ and $r = 28$).

The fixed points of system (1) and their corresponding stabilities depend on r . For $r \leq 1$ there is only one (stable) fixed point in $(0, 0, 0)$. For $r > 1$ the origin loses its stability and a pair of new fixed points appear: $(\pm[b(r-1)]^{1/2}, \pm[b(r-1)]^{1/2}, r-1)$, which are stable in the range $1 < r \leq r_c$ with $r_c = \sigma(\sigma + b + 3)/(\sigma - b - 1)$. (Note that the critical value r_c exists if and only if $\sigma > b + 1$). For $r > r_c$ all fixed points are unstable, and the Lorenz system can exhibit either periodic or chaotic behavior (see, e.g., Ref. [20] for a comprehensive exposition on the matter).

Since we are interested in the case $r > 1$, we can suitably define the scaled coordinates $x = X/[b(r-1)]^{1/2}$, $y = Y/[b(r-1)]^{1/2}$, $z = Z/(r-1)$, so that the system (1) becomes

$$\begin{cases} \dot{x} = \sigma(y - x) \\ \dot{y} = -y + x + (r-1)(1-z)x \\ \dot{z} = b(xy - z) \end{cases} \quad (2)$$

with fixed points $(0, 0, 0)$ and $(\pm 1, \pm 1, 1)$.

We now reduce the Lorenz system to a unique differential equation for $x = x(t)$, whose solution makes it possible the direct calculation of $y(t)$ and $z(t)$. By inserting into the third equation of (2) the expression for y in terms of x obtained from the first, one easily gets

$$\dot{z} + bz = \frac{b}{2\sigma} \left[\frac{d}{dt}(x^2) + 2\sigma x^2 \right], \quad (3)$$

whose general solution is given by

$$z(t) = e^{-b(t-t_0)} \left(z(t_0) - \frac{b}{2\sigma} x^2(t_0) \right) + \frac{b}{2\sigma} x^2(t) + \left(1 - \frac{b}{2\sigma} \right) b \int_{t_0}^t ds e^{-b(t-s)} x^2(s). \quad (4)$$

We have already stated that we are interested in the evolution of the Lorenz system in the chaotic steady state, i.e. far from the initial transient. Thus, we let t_0 move back to $-\infty$ and obtain the steady-state expression for $z(t)$, which can be written in the form

$$z(t) = \frac{b}{2\sigma}x^2(t) + \left(1 - \frac{b}{2\sigma}\right) [x^2]_b(t), \quad (5)$$

where we use the square brackets notation $[f]_k(t)$ to indicate the exponential average of any suitable time function f on its past history:

$$[f]_k(t) \equiv k \int_0^\infty ds e^{-ks} f(t-s). \quad (6)$$

From now on we shall refer to $[f]_k$ as the *k-exponentially vanishing memory* of the function f or in short its *memory*. Note that, for the memory $[f]_k$ to exist, it suffices that $f(t) \simeq O(\exp(-ht))$, with $h < k$, as $t \rightarrow -\infty$ (the time functions we shall be dealing with are even bounded in this limit).

To summarize, we insert in the second equation of (2) $y(t)$ obtained from the first equation and $z(t)$ given by (5) and get for the variable $x = x(t)$ alone in chaotic steady state the following second order differential equation with memory (in fact, an integral-differential equation)

$$\ddot{x} + (\sigma + 1)\dot{x} + \sigma(r - 1) \left(\frac{b}{2\sigma}(x^2 - 1)x + \left(1 - \frac{b}{2\sigma}\right) [x^2 - 1]_b x \right). \quad (7)$$

One can interpret the previous equation as the dynamical equation of a (unit mass) particle, viscously moving in a compound potential energy field consisting of a weighted average (in the chaotic regime $b/2\sigma < 1$) of a quartic potential energy field independent of time (Fig. 1)

$$U(x) = \sigma(r - 1) \frac{(x^2 - 1)^2}{4} \quad (8)$$

and of a quadratic potential energy field

$$U_t(x) = \sigma(r - 1) [x^2 - 1]_b \frac{(x^2 - 1)}{2}, \quad (9)$$

whose curvature is given by a suitable memory function of the past motion.

Without the memory term the particle would stop in one of the minima of the bistable potential U due to the damping term $-(\sigma + 1)\dot{x}$. Indeed, the U_t contribution yields, through an exponential average on the past evolution, an “endogenous” forcing term which can permanently sustain the motion. The particle oscillates with growing amplitude around the minimum of one of the potential well until its energy is sufficient to allow the crossing of the barrier in $x = 0$. As already said, the chaotic behavior of the system emerges just in the unpredictability of the instant at which the particle moves from one well to the other. Trajectories relative to very slightly different initial conditions can produce strongly different sequences in the number of oscillations in each well. In the next section we shall explain this fact analytically.

In order to simplify and to make the analysis standard, let us rescale the time t in Eq. (7) as $t \rightarrow \tau \equiv [(r-1)b/2]^{1/2} t$, to obtain the equation (hereafter called *Lorenz equation*)

$$\frac{d^2x}{d\tau^2} + \eta \frac{dx}{d\tau} + (x^2 - 1)x = -\alpha[x^2 - 1]_\beta x, \quad (10)$$

where

$$\eta = \frac{\sigma + 1}{\sqrt{(r-1)b/2}}, \quad \alpha = \frac{2\sigma}{b} - 1, \quad \beta = \sqrt{\frac{2b}{r-1}}.$$

Note that, given b and r , σ (the viscosity parameter in the original problem) affects both the friction term and the forcing term in the Lorenz equation. This fact shows how much these “opposite” contributions are in fact strictly related if the equation is to be viewed as representative of the original Lorenz system. Even if one now considers the Lorenz equation as the main subject of the study, one must note that not all the (positive) values of α , β , η are consistent with their definition in terms of the original parameters b , σ , r . In particular, in order to observe chaotic behavior, the following inequality must hold

$$\alpha > \frac{\eta(2 + \beta(\beta + \eta))}{2\beta}. \quad (11)$$

(Further details on the relation between the two sets of parameters are given in Appendix A).

Equation (10) allows us to highlight the role of the memory forcing term in the Lorenz system dynamics. For this purpose it is interesting to compare the Lorenz equation with other examples of chaotic nonlinear (nonautonomous) systems as, for instance, the inverse Duffing equation $\ddot{x} + \eta\dot{x} + (x^2 - 1)x = A \cos(\Omega t)$, which describes a sinusoidally forced quartic oscillator [21], or more appropriately the parametrically forced equation

$$\ddot{x} + \eta\dot{x} + (x^2 - 1)x = -A \cos(\Omega t) x. \quad (12)$$

Note that in the latter cases the motion is sustained by externally assigned forcing terms, while in the case of the Lorenz equation the motion is self-sustained by the endogenous term $-\alpha[x^2 - 1]_\beta x$. In Figs. 2 and 3 we give a numerically obtained comparison between the phase portraits of the Lorenz equation and of equation (12) with parameters (α, β, η) , and (A, Ω) suitably chosen in order to get similar ranges of motion. Note that the endogenous Lorenz forcing term, mimed by $-A \cos(\Omega t) x$, is in fact neither monochromatic nor with vanishing average value.

III. THE GENERALIZED LORENZ SYSTEM

The Lorenz equation (10) can be usefully recast in the form

$$\frac{d^2x}{d\tau^2} + \eta \frac{dx}{d\tau} + \left(q(x) + \alpha [q(x)]_\beta \right) \Phi'(x) = 0 \quad (13)$$

where the prime indicates the derivative with respect to x and in our case $\Phi(x) = 1/2 x^2$ and $q(x) = x^2 - 1$. Such an equation can be interpreted as the description of the motion of

a unit mass particle subjected to a viscous force $-\eta dx/d\tau$ and interacting with a potential field Φ through a “dynamically varying charge” $q_\tau(x) = q(x) + \alpha[q(x)]_\beta$. This charge both depends on the instantaneous particle position $x(\tau)$ (by means of the term $q(x)$) and on the past evolution (by means of the *memory charge* $[q(x)]_\beta$). The coupling of $[q]_\beta$ with the fixed potential field Φ acts as an endogenous forcing term which can sustain the motion even in the presence of friction, and the chaotic behavior can actually arise from the synergy between this term and the viscosity.

Put in the form (13), the Lorenz equation is arranged to be generalized to a generic charge $q(x)$ interacting with a generic potential field $\Phi(x)$. Correspondingly, it is possible to obtain a *generalized Lorenz system* whose “ x - projection” (far from the initial transient) yields Eq. (13). Indeed, by inverting the calculation followed to derive Eq. (13) from system (2), one easily gets the generalized Lorenz dynamical system

$$\begin{cases} \dot{x} = \sigma(y - x) \\ \dot{y} = -y + x + (r - 1)(1 - z) \Phi'(x) \\ \dot{z} = -bz + b[\frac{1}{2}q'(x)(y - x) + q(x) + 1]. \end{cases} \quad (14)$$

Therefore, the specific Lorenz model can be viewed as singled out from a quite general class of dynamical systems which can exhibit chaotic behavior, their common essential property being an exponentially vanishing memory effect together with a viscous damping.

Equations (13) and (14) are related to Eq. (7) by assuming as potential energy field the quantity $\mathcal{U} = (b/2\sigma)U + (1 - b/2\sigma)U_t$ with

$$U = \sigma(r - 1) \int q(x) \Phi'(x) dx \quad \text{and} \quad U_t = \sigma(r - 1)[q]_\beta \Phi. \quad (15)$$

Obviously, any choice of q and Φ should maintain the main properties of the Lorenz model, i.e., correspond to a two-well piecewise differentiable potential energy $U(x)$, such that $U(x) \rightarrow \infty$ as $|x| \rightarrow \infty$.

We shall now focus our attention on a particular choice for q and Φ , that will maintain all the qualitative properties of the Lorenz system and, at the same time, will allow us to deal with chaos analytically.

IV. THE PIECEWISE LINEARIZED LORENZ SYSTEM

A. Linearization near fixed points

As already noticed, the chaotic behavior of the Lorenz system essentially depends on the unpredictability of the instants when x change its sign: as long as it keeps constant sign the system evolution is certainly nonlinear, and nevertheless not “chaotic” at all. This fact suggests a slight modification of the original form of the Lorenz system, in order to single out analytically the origin of chaos without to be faced with the difficulties arising from nonlinear features. We thus set in Eqs. (13) and (14) $\Phi(x) = |x|$ and $q(x) = |x| - 1$ obtaining (for $x \neq 0$) the piecewise linear Lorenz-like equation

$$\frac{d^2x}{d\tau^2} + \eta \frac{dx}{d\tau} + \left\{ |x| - 1 + \alpha [|x| - 1]_\beta \right\} \text{sgn}(x) = 0, \quad (16)$$

where $\text{sgn}(x) \equiv |x|/x$. The corresponding piecewise linearized dynamical system, with the original choice of parameters, is then given by

$$\begin{cases} \dot{x} = \sigma(y - x) \\ \dot{y} = -y + x + (r - 1)(1 - z) \text{sgn}(x) \\ \dot{z} = -bz + b \text{sgn}(x) \frac{x + y}{2}. \end{cases} \quad (17)$$

Our assumptions on Φ and q correspond in Eq. (7) to $U(x) = \sigma(r - 1)(|x| - 1)^2/2$ and $U_t(x) = \sigma(r - 1)[|x| - 1]_b(|x| - 1)$. Thus, we are faced with a simplified model, obtained by replacing the constant-in-time quartic potential with a piecewise quadratic one resulting from the superposition of two parabolas with vertex in ± 1 and truncated at $x = 0$ (Fig. 4). The two-well character of U is obviously maintained as well as the piecewise differentiability. The replacement of the original potential actually corresponds to a linearization of the system around both unstable fixed points $(\pm 1, \pm 1, 1)$, with the matching performed in $x = 0$. It appears that the chaotic behavior of the original model does not depend on the differentiability in $x = 0$. One can guess that also other classes of dynamical systems can be transformed in a piecewise linearized version by means of the same operations.

It is easy to check that the fixed points of (17) are $(\pm 1, \pm 1, 1)$ and that the equation ruling their local stability is the same as for the original Lorenz system with parameters b , σ , $\rho \equiv (r + 1)/2$. In particular, if $\sigma > b + 1$, the critical value of r for our piecewise linear system (17) is given by $r_c^{(lin)} = 2r_c - 1$. In Figs. 5 and 6 two chaotic phase portrait for systems (2) and (17) are shown, corresponding to the same choice of b and σ , and different choices of r in order to preserve the relationships between r and the proper corresponding critical value.

When dealing with system (17), the main simplification is that it is separately linear for $x < 0$ and $x > 0$ and can thus be analytically solved in each region. Indeed, by applying the operator $(d/d\tau + \beta)$ to each side of Eq. (16) one obtains the equation

$$\frac{d^3x}{d\tau^3} + (\beta + \eta)\frac{d^2x}{d\tau^2} + (1 + \beta\eta)\frac{dx}{d\tau} + \beta(1 + \alpha)(x - \text{sgn}(x)) = 0, \quad (18)$$

which can be explicitly solved separately on each side of $x = 0$. The nonlinearity of the model is simply reduced to a change of sign of the forcing term $\pm\beta(1 + \alpha)$ when x crosses the plane $x = 0$, henceforth denoted with π [22]. As we shall see, the crossing times are somewhat unpredictable, as they result from the discontinuous solutions of an (incidentally transcendental) equation. Our piecewise linearized system will thus turn out to be an important tool to analytically investigate the emergence of chaos in Lorenz-like systems. The main advantage of the piecewise linearization is that one has to deal only with the simplest nonlinearity, i.e. an isolated (not eliminable) discontinuity (see, e.g., Refs. [23–27] for other examples of piecewise linear chaotic dynamical systems).

B. Analysis of the motion

Let us now consider in detail the second order integral-differential equation (16), which describes the evolution in time of x for the piecewise linearized system in the chaotic steady

state. It is equivalent to a third order nonlinear differential equation whose phase space is described by the coordinates x, \dot{x}, \ddot{x} (with a small abuse of notation from this time on we shall indicate with the dot the differentiation with respect to τ). Solutions of Eq. (16) can be easily calculated with tools of the customary analysis on each side of $x = 0$. To obtain a global solution, such partial solutions should be matched at $x = 0$ under the reasonable assumptions that the position x , the velocity \dot{x} , and the memory $[|x|]_\beta$ are continuous [28]. Notice that, in contrast, when crossing the plane π , the acceleration \ddot{x} turns out to be undefined. However, if $x(\tilde{\tau}) = 0$, referring to the left and right time limits $\ddot{x}(\tilde{\tau}^-)$ and $\ddot{x}(\tilde{\tau}^+)$, it appears from Eq. (16) that they are related by the equation $\ddot{x}(\tilde{\tau}^-) + \ddot{x}(\tilde{\tau}^+) = -2\eta \dot{x}(\tilde{\tau})$. In the sequel we shall refer to $\ddot{x}(\tilde{\tau}^-)$ and $\ddot{x}(\tilde{\tau}^+)$ as the acceleration “immediately” before and “immediately” after the crossing, respectively.

Since Eq. (16) is invariant under the transformation $x \rightarrow -x, \tau \rightarrow \tau$, we can focus our attention only on one of the two regions, e.g. $x > 0$, and describe the motion in this half-space (the evolution in its twin half-space being recovered through the change $x \rightarrow -x$). Clearly, this is equivalent to put a “rigid wall” in $x = 0$ and look at the crossing of π as an elastic collision.

In summary, according to the previous scheme, the system evolution in time is completely described by the following steps:

1. motion for $x > 0$;
2. collision against π and discontinuity of \ddot{x} ;
3. inversion $x \rightarrow -x$ and matching with a new solution defined in the region $x > 0$ again.

1. Motion in the half-space $x > 0$

If we define $\xi \equiv x - 1$, Eq. (18) assume a simple form

$$\ddot{\xi} + (\beta + \eta)\dot{\xi} + (1 + \beta\eta)\dot{\xi} + \beta(1 + \alpha)\xi = 0, \quad (19)$$

that is a linear third order differential equation (homogeneous and with constant coefficients). As a consequences of the Routh-Hurwitz theorem [29], a critical value α_c for the parameter α exists, i.e.

$$\alpha_c = \frac{(1 + \beta\eta)(\beta + \eta)}{\beta} - 1. \quad (20)$$

For $\alpha > \alpha_c$ the fixed points are unstable saddle focus with a real negative eigenvalue $-\lambda_0$ and a pair of complex conjugates eigenvalues $\lambda_1 = \lambda_r + i\lambda_i, \bar{\lambda}_1 = \lambda_r - i\lambda_i$.

For the sake of simplicity we shall indicate with $(0, \tau_1)$ the time interval between two consecutive collisions in the steady-state of the system. Without loss of generality we assume $x = 0$ and $\dot{x} > 0$. Then, it can be easily shown that in the time interval $(0, \tau_1)$ the motion in the phase space $\xi, \dot{\xi}, \ddot{\xi}$ ($\xi > -1$) is completely described by the equation

$$\boldsymbol{\xi}(\tau) = \mathcal{M}(\tau) \mathcal{M}(0)^{-1} \boldsymbol{\xi}_0, \quad (21)$$

where we have defined

$$\boldsymbol{\xi}(\tau) \equiv \begin{pmatrix} \xi(\tau) \\ \dot{\xi}(\tau) \\ \ddot{\xi}(\tau) \end{pmatrix}, \quad \boldsymbol{\xi}_0 \equiv \begin{pmatrix} \xi_0 \\ \dot{\xi}_0 \\ \ddot{\xi}_0 \end{pmatrix} \equiv \begin{pmatrix} -1 \\ \dot{\xi}(0) \\ \ddot{\xi}(0^+) \end{pmatrix},$$

and

$$\mathcal{M}(\tau) = \begin{pmatrix} \operatorname{Re}(e^{\lambda_1 \tau}) & \operatorname{Im}(e^{\lambda_1 \tau}) & e^{-\lambda_0 \tau} \\ \operatorname{Re}(\lambda_1 e^{\lambda_1 \tau}) & \operatorname{Im}(\lambda_1 e^{\lambda_1 \tau}) & -\lambda_0 e^{-\lambda_0 \tau} \\ \operatorname{Re}(\lambda_1^2 e^{\lambda_1 \tau}) & \operatorname{Im}(\lambda_1^2 e^{\lambda_1 \tau}) & \lambda_0^2 e^{-\lambda_0 \tau} \end{pmatrix}.$$

(Note that, for $\alpha > \alpha_c$, $\mathcal{M}(0)$ is always invertible since $\det \mathcal{M}(0) = \lambda_i [\lambda_i^2 + (\lambda_r + \lambda_0)^2]$ and $\lambda_i > 0$). The eigenvalues of the matrix $\mathcal{M}(\tau) \mathcal{M}(0)^{-1}$, which connects the vector $\boldsymbol{\xi}(\tau)$ to its initial value $\boldsymbol{\xi}_0$, are $e^{\lambda_1 \tau}$, $e^{\bar{\lambda}_1 \tau}$, $e^{-\lambda_0 \tau}$, with corresponding (constant-in-time) eigenvectors

$$\mathbf{v}_1 \equiv \begin{pmatrix} 1 \\ \lambda_1 \\ \lambda_1^2 \end{pmatrix}, \quad \mathbf{v}_2 \equiv \begin{pmatrix} 1 \\ \bar{\lambda}_1 \\ \bar{\lambda}_1^2 \end{pmatrix}, \quad \mathbf{v}_3 \equiv \begin{pmatrix} 1 \\ -\lambda_0 \\ \lambda_0^2 \end{pmatrix}.$$

With respect to the base $\{\mathbf{v}_1, \mathbf{v}_2, \mathbf{v}_3\}$ one has

$$\boldsymbol{\xi}(\tau) = e^{\lambda_r \tau} (c_1 e^{\lambda_i \tau} \mathbf{v}_1 + c_2 e^{-\lambda_i \tau} \mathbf{v}_2) + c_3 e^{-\lambda_0 \tau} \mathbf{v}_3. \quad (22)$$

For the saddle point $\boldsymbol{\xi} = \mathbf{0}$ there exist a stable one-dimensional manifold \mathcal{W}^s corresponding to \mathbf{v}_3

$$\mathcal{W}^s = \{p \mathbf{v}_3 \mid p > -1\}$$

and an unstable two-dimensional manifold \mathcal{W}^u generated by $\mathbf{v}_1, \mathbf{v}_2$ (see Fig. 7)

$$\mathcal{W}^u = \left\{ p \frac{\mathbf{v}_1 + \mathbf{v}_2}{2} + q \frac{\mathbf{v}_1 - \mathbf{v}_2}{2i} \mid p > -1, q \in \mathbb{R} \right\}.$$

The evolution of the linearized system in the interval $(0, \tau_1)$ is the combination of an exponential decay along \mathcal{W}^s and of an amplified rotation on \mathcal{W}^u . To determine the relative quickness of each component of the motion with respect to the other, consider that from Eq. (19) it is easily checked that $\lambda_0 - 2\lambda_r = \beta + \eta$, and so $\lambda_0 > \lambda_r \forall \alpha, \beta, \eta$. Therefore, the exponential decay along the stable manifold \mathcal{W}^s is always more rapid than the exponential oscillating growth on the unstable manifold \mathcal{W}^u , the parameter controlling this difference being $\beta + \eta$.

Although the fixed points are saddle focus, it appears that the piecewise linearized system does not exhibit Shilnikov chaos [30] owing to the absence of an homoclinic orbit.

2. π -collision and inversion

To complete the description of the piecewise linearized system dynamics, we consider the instant τ_1 at which the first collision occurs. At this time, as already remarked, the trajectory coming from the half-space $x > 0$ must be matched with the solution defined again in the same region, but with corresponding new “initial conditions” [31]

$$\begin{cases} \xi_1 = -1 \\ \dot{\xi}_1 = -\dot{\xi}(\tau_1) \\ \ddot{\xi}_1 = -\ddot{\xi}(\tau_1^+) = \ddot{\xi}(\tau_1^-) + 2\eta \dot{\xi}(\tau_1), \end{cases} \quad (23a)$$

or, in matrix form,

$$\boldsymbol{\xi}_1 = \mathfrak{J} \mathcal{D} \boldsymbol{\xi}(\tau_1^+) \quad (23b)$$

with

$$\mathcal{D} \equiv \begin{pmatrix} 1 & 0 & 0 \\ 0 & 1 & 0 \\ 0 & -2\eta & -1 \end{pmatrix} \quad \text{and} \quad \mathfrak{J} \equiv \begin{pmatrix} 1 & 0 & 0 \\ 0 & -1 & 0 \\ 0 & 0 & -1 \end{pmatrix}.$$

The matrix \mathcal{D} accounts for the acceleration discontinuity in $x = 0$, while \mathfrak{J} yields the sign inversion after the impact. From Eqs. (21) and (23b) it follows that the velocity and the acceleration immediately after the collision are related to the initial conditions by the operator $\mathcal{P}(\tau) \equiv \mathfrak{J} \mathcal{D} \mathcal{M}(\tau) \mathcal{M}(0)^{-1}$, according to the formula

$$\boldsymbol{\xi}_1 = \mathcal{P}(\tau_1(\boldsymbol{\xi}_0)) \boldsymbol{\xi}_0. \quad (24)$$

Notice the highlighted dependence of τ_1 on $\boldsymbol{\xi}_0$, which reveals the nonlinear character of this important relationship.

Starting from the above results, the very origin of chaos in the piecewise linearized Lorenz system will be identified and discussed in the next section. We shall also show that the basic mechanisms for chaos to emerge apply also to the original Lorenz system.

C. Dependence of τ_1 on initial conditions

1. Unpredictability of the crossing time

As already observed, the instant at which the plane π is crossed, strongly depends on the initial conditions. This fact is strictly related to the chaotic behavior of Lorenz-like systems. Let us now study in some detail this topic for the piecewise linearized model.

The instant τ_1 at which the first collision occurs is defined by the condition $\xi(\tau_1) = -1$. From the first line of Eq. (21) τ_1 is thus the smallest positive solution of the transcendental equation

$$-1 = C_1 e^{\lambda_r \tau_1} \cos(\lambda_i \tau_1) + C_2 e^{\lambda_r \tau_1} \sin(\lambda_i \tau_1) + C_3 e^{-\lambda_0 \tau_1} \quad (25)$$

where C_1, C_2, C_3 are linearly related to initial conditions. The *residence time* τ_1 is therefore the first intersection of the graphs of $g(\tau_1) = -C_3 e^{-\lambda_0 \tau_1} - 1$ and $h(\tau_1) = C_1 e^{\lambda_r \tau_1} \cos(\lambda_i \tau_1) + C_2 e^{\lambda_r \tau_1} \sin(\lambda_i \tau_1)$. Since g is a decreasing exponential function and h an oscillating function with growing amplitude, one can easily understand why even a little modification of initial conditions can produce a discontinuous variation of τ_1 (Fig. 8).

In conclusion, the unpredictability of the residence time is closely connected to the discontinuous character of the solutions of Eq. (25). The chaotic behavior for the the piecewise linearized system clearly stems from such unpredictability. Our claim is that an entirely analogous situation exists also for the original Lorenz model. We shall return however in more detail on this important analogy in the sequel.

2. The residence time τ_1 as a function of $\dot{\xi}_0$ and $\ddot{\xi}_0$

We now explicitly investigate the dependence of τ_1 on the initial velocity and acceleration. As previously remarked, the function $\tau_1 = \tau_1(\dot{\xi}_0, \ddot{\xi}_0)$ is implicitly defined as the smallest positive solution of Eq. (25). Since C_1, C_2, C_3 are linearly related to the initial conditions, Eq. (25) can be rewritten in terms of $\dot{\xi}_0$ and $\ddot{\xi}_0$. In this form it describes a family \mathcal{S} of straight lines in the plane $\{\dot{\xi}_0, \ddot{\xi}_0\}$ parametrized by τ_1

$$\mathcal{S} : \quad A(\tau_1) \dot{\xi}_0 + B(\tau_1) \ddot{\xi}_0 + C(\tau_1) = 0 \quad (26)$$

[see Appendix B for the explicit expression of the coefficients $A(\tau_1), B(\tau_1), C(\tau_1)$].

Let us denote with $(T_i), i \geq 0$ the ordered sequence of the zeros of $B(\tau_1)$. Note that one always has $T_0 = 0$. The slope of the straight lines of \mathcal{S} , $-A/B$, and their ordinate for $\dot{\xi}_0 = 0$, i.e. $-C/B$, have their singularities in $T_i, i \geq 0$. Both these functions are only asintotically periodic because of the presence of terms proportional to $e^{-\lambda_0 \tau_1}$, which become negligible only for large τ_1 (Figs. 9 and 10).

In each interval $(T_i, T_{i+1}), i \geq 0$, the function $-A/B$ is everywhere growing (see Appendix B) and varies from $-\infty$ and $+\infty$. Therefore, as τ_1 increases, the straight lines of \mathcal{S} rotate anticlockwise and at the same time translate starting from the $\ddot{\xi}_0$ -axis (obtained for $\tau_1 = 0$) (Fig. 11).

The envelope of the family \mathcal{S} is a curve

$$\gamma : \begin{cases} \dot{\xi}_0 = \dot{\xi}_0(\tau_1) \\ \ddot{\xi}_0 = \ddot{\xi}_0(\tau_1) \end{cases}$$

which looks similar to an elliptic spiral (Fig. 12). (A parametrical representation of γ is given in Appendix B).

From Eq. (26) the contour lines of the function τ_1 are parts of straight lines in the plane $(\dot{\xi}_0, \ddot{\xi}_0)$. Indeed, according to the definition, each line of \mathcal{S} is in fact a contour line for τ_1 only where its points do not belong to another line corresponding to a smaller value of τ_1 and, furthermore, only where their abscissas correspond to positive values of $\dot{\xi}_0$. Rather than a family of straight lines, the function contour lines are raies or segments according to the constant value of τ_1 .

For τ_1 ranging from 0 to T_2 these lines perform a complete anticlockwise “rotation,” starting

from the $\ddot{\xi}_0$ -axis. Thus, they cover the entire half-plane $\dot{\xi}_0 \geq 0$ except the region inside their envelope; from this first rotation one obtains a set of raies (Fig. 13).

Subsequently, for τ_1 ranging from T_2 to T_4 the contour lines become segments of variable orientation and contained in the region delimited by the curve already generated from the first rotation and the new envelope of the second set of straight lines. This behavior repeats itself $\forall \tau_1 \in [T_{2i}, T_{2i+1}]$, $i \geq 0$. Because of the aperiodic character of the functions involved, the curve γ outlines in the positive half-plane a structure consisting of “pseudo-elliptic” annula. Moving anticlockwise along each of these annula, τ_1 grows continuously. On the contrary, passing through the border that separates two different bands, one meets discontinuities in the dependence of τ_1 on initial conditions.

The curve γ “winds” round the point $P_0 \equiv (\lambda_0, -\lambda_0^2)$ (see Fig. 12). For $(\dot{\xi}_0, \ddot{\xi}_0) \rightarrow (\lambda_0, -\lambda_0^2)$ one has $\tau_1 \rightarrow \infty$, since for these initial conditions one obtains $C_1 = C_2 = 0$ and the system exactly lies on the stable manifold \mathcal{W}^s . Its motion is in this case an exponential decay towards the fixed point $\boldsymbol{\xi} = \mathbf{0}$.

The previous observations allow to easily guess the structure of the graph of $\tau_1 = \tau_1(\dot{\xi}_0, \ddot{\xi}_0)$ shown in Fig. 14. It should be noted that τ_1 shows instability with respect to the initial conditions only in a limited subset of the half-plane $\dot{\xi}_0 \geq 0$. As we shall see, it is natural to expect that in the chaotic regime the system is quickly attracted inside this region.

D. The piecewise linearized model as a one-dimensional map

1. The π -plane Poincaré map

At this point of our study we have analyzed in some detail the unpredictability of the time at which the system crosses the plane π . To completely motivate the chaotic dynamics of the piecewise linearized system and thus of the original model, we must, however, add some further results on the attracting set of the system.

All results obtained in the previous section can be easily extended to the n -th collision against π . Specifically, denoting with $\boldsymbol{\xi}_n$ the array assigning position, velocity, and acceleration immediately after the n -th collision

$$\boldsymbol{\xi}_n \equiv \begin{pmatrix} -1 \\ \dot{\xi}_n \\ \ddot{\xi}_n \\ \xi_n \end{pmatrix},$$

we have [similarly to Eq. (24)]

$$\boldsymbol{\xi}_n = \mathcal{P}(\tau_n) \boldsymbol{\xi}_{n-1}, \quad (27)$$

where we have denoted with τ_n the n -th residence time, i.e., the time interval between the $(n-1)$ -th collision and the n -th one.

The first line of Eq. (27) gives τ_n in terms of $\dot{\xi}_{n-1}$ and $\ddot{\xi}_{n-1}$: the dependence of this time on the $(n-1)$ -th initial conditions has already been discussed in Section IV C 2. Knowing τ_n , the other two lines allow to relate the velocity $\dot{\xi}_n$ and the acceleration $\ddot{\xi}_n$ to $\dot{\xi}_{n-1}$ and $\ddot{\xi}_{n-1}$. Eq. (27) defines a two-dimensional first-return Poincaré map between $(\dot{\xi}_n, \ddot{\xi}_n)$ and $(\dot{\xi}_{n-1}, \ddot{\xi}_{n-1})$, obtained from the section $\xi = -1$ of the phase space $\xi, \dot{\xi}, \ddot{\xi}$. We recall that, in

spite of its appearance, the map (27) is in fact non-linear, since the matrix \mathcal{P} depends on τ_n , which is a transcendental discontinuous function of the $(n - 1)$ -th initial conditions. Indeed, under suitable conditions, the two-dimensional map for the linearized system practically reduces to a one-dimensional map.

2. Approximation of the system with a one-dimensional map

It has been already shown that for $\xi > -1$ the motion in the phase space has the form (22)

$$\boldsymbol{\xi}(\tau) = c_1 e^{\lambda_1 \tau} \mathbf{v}_1 + c_2 e^{\bar{\lambda}_1 \tau} \mathbf{v}_2 + c_3 e^{-\lambda_0 \tau} \mathbf{v}_3$$

where λ_0 and $\lambda_r = \text{Re}(\lambda_1)$ satisfy the equation $\lambda_0 - 2\lambda_r = \beta + \eta$, which in turn implies $\lambda_0 > \lambda_r$. As a consequence the evolution in the phase space $\xi, \dot{\xi}, \ddot{\xi}$ consists both of a “rapid” decay towards $\boldsymbol{\xi} = \mathbf{0}$ along the stable manifold \mathcal{W}^s and of a “slow” amplified oscillation on \mathcal{W}^u . We thus expect the phase trajectories to be strongly attracted on the unstable manifold and, once on \mathcal{W}^u , to slowly spiral outwards. Provided trajectories start close enough to \mathcal{W}^u , then they meet the π -plane very close to its intersection with \mathcal{W}^u itself, i.e., along the straight line

$$\mathcal{L}^- : \begin{cases} \ddot{\xi} + 2\lambda_r \dot{\xi} + (\lambda_r^2 + \lambda_i^2) = 0 \\ \xi = -1. \end{cases} \quad (28)$$

Let us assume that the attraction towards the unstable manifold is very strong and thus it takes place almost instantaneously (the goodness of this assumption is controlled by $\beta + \eta$). Under this hypothesis all trajectories approximately hit π along the straight line \mathcal{L}^- . Thus, from Eq. (23b), it follows that, immediately after each collision, the system necessarily lies very close to the straight line

$$\mathcal{L}^+ : \begin{cases} \ddot{\xi} + 2(\eta + \lambda_r)\dot{\xi} - (\lambda_r^2 + \lambda_i^2) = 0 \\ \xi = -1. \end{cases} \quad (29)$$

Therefore, the following relation between velocity and acceleration is expected to approximately hold

$$\ddot{\xi}_n + 2(\eta + \lambda_r)\dot{\xi}_n - (\lambda_r^2 + \lambda_i^2) = 0. \quad (30)$$

From Eqs. (16) and (30) an analogous linear dependence between the velocity and the memory follows

$$(\eta + 2\lambda_r)\dot{\xi}_n - \alpha w_n + 1 - (\lambda_r^2 + \lambda_i^2) = 0, \quad (31)$$

where w_n denotes the β -memory of ξ evaluated at the n -th collision. As a consequence, in the limit we have considered, the attracting set for the map (27) is \mathcal{L}^+ and, therefore, it reduces to an one-dimensional map.

Since in the chaotic steady-state the velocity and the acceleration that define the initial conditions for the trajectory after each impact are not independent, the time τ_n can be

expressed as a function of $\dot{\xi}_{n-1}$ alone: $\tau_n = \tau_n(\dot{\xi}_{n-1})$ (see Fig. 15). The behavior of this map is easily understood if we refer to the graph of τ_1 as a functions of $\dot{\xi}_0$ and $\ddot{\xi}_0$ (see Fig. 14). Indeed, in the chaotic regime \mathcal{L}^+ is superimposed to the region of the plane $(\dot{\xi}_{n-1}, \ddot{\xi}_{n-1})$ contained by γ , where τ_1 shows unstable behavior with respect to a change in the initial conditions (Fig. 16). For those values of $\dot{\xi}_{n-1}$, for which \mathcal{L}^+ passes through the same “pseudo-elliptic” corona, τ_n slowly changes with varying crossing velocity. On the contrary, when \mathcal{L}^+ intersects the boundary between two different coronas, τ_n shows a discontinuity in its dependence on $\dot{\xi}_{n-1}$ (Fig. 15).

The linear dependence between velocity and acceleration immediately after each collision implies that the Poincaré map (27) becomes one-dimensional, e.g. a map between $\dot{\xi}_n$ and $\dot{\xi}_{n-1}$. Figure 17 shows this fact for $\alpha = 6.50$, $\beta = 0.19$, $\eta = 0.78$. By simple inspection of the derivatives corresponding to the fixed points of the map one can easily check that they are all unstable, so that the map produces a chaotic behavior. Note that the discontinuities simply correspond to the analogous ones in the function $\tau_n = \tau_n(\dot{\xi}_{n-1})$, evaluated along the straight line given by (30) and drawn in Fig.16.

For the sake of completeness, we turn now to the description of the piecewise linearized system in the original phase space x, \dot{x}, \ddot{x} . There the system has two fixed points $(\pm 1, 0, 0)$. For each one there exists a stable manifold

$$\mathcal{W}_{\pm}^s = \{p \mathbf{v}_3 + (\pm 1, 0, 0) \mid p \gtrless \mp 1\} \quad (32)$$

and an unstable manifold

$$\mathcal{W}_{\pm}^u = \left\{ p \frac{\mathbf{v}_1 + \mathbf{v}_2}{2} + q \frac{\mathbf{v}_1 - \mathbf{v}_2}{2i} + (\pm 1, 0, 0) \mid p \gtrless \mp 1 \text{ and } q \in \mathbb{R} \right\}. \quad (33)$$

During the evolution the trajectories are rapidly attracted on the unstable manifold relative to the half-plane where they belong (Fig. 18). Thus, immediately after the crossing of the π -plane the phase point lies on one of the straight lines

$$\begin{cases} \ddot{x} + 2(\eta + \lambda_r)\dot{x} + (\lambda_r^2 + \lambda_i^2) \operatorname{sgn}(\dot{x}) = 0 \\ x = 0, \end{cases}$$

while the memory and the velocity are linearly related according to equation

$$(\eta + 2\lambda_r) \dot{x}_n - \alpha \operatorname{sgn}(\dot{x}_n) w_n + 1 - (\lambda_r^2 + \lambda_i^2) = 0. \quad (34)$$

As for the crossing of the π -plane, the system can therefore be described by a one-dimensional map. To get the maps $\tau_n = \tau_n(\dot{x}_{n-1})$ and $\dot{x}_n = \dot{x}_n(\dot{x}_{n-1})$ from the analogous ones in the rigid wall scheme, one has simply to consider that ξ_n coincides with $|\dot{x}_n|$.

The reader should note that all the maps we have drawn in the previous figures have been obtained by numerically solving the analytical equation (27), which exactly defines τ_n , $\dot{\xi}_{n+1}$, and $\ddot{\xi}_{n+1}$, and they have not been computed by numerical integration of the differential system (as usual for non solvable dynamical systems like the Lorenz original one). Thus, the use of numerical tools has been required only because of the transcendental character of the concerned equation.

We explicitly remark that in general the attraction towards \mathcal{W}^u is not infinite, but nevertheless more rapid than the amplified rotation on the unstable manifold (remember that $\lambda_0 - 2\lambda_r = \beta + \eta > 0 \forall \alpha, \beta, \eta$). Therefore, we can expect that, if $\beta + \eta$ is finite, the attractor set is not exactly the straight line \mathcal{L}^+ , but a narrow “strip” that contains \mathcal{L}^+ . This strip intersects the region of the graph of τ_n where the residence time is strongly dependent on initial conditions and the mechanism for chaos to arise is absolutely the same. Our numerical simulations for finite $\beta + \eta$ are in excellent agreement with these predictions and then we do not show their corresponding graphs here, since they are practically indistinguishable from the graphs we have already discussed.

V. COMPARISON WITH THE ORIGINAL LORENZ SYSTEM

We conclude our analysis by showing some simulated numerical results. Before doing that, some remarks are worth discussing. We previously considered x, \dot{x}, \ddot{x} as independent coordinates in the phase space because of their physical meaning: it is more intuitive to speak about acceleration rather than of memory of the system. Unfortunately, if we want to “assign initial conditions” to the original Lorenz system after the crossing of the plane π , we cannot consider the acceleration and the velocity since from Eq. (10) they are not independent variables in $x = 0$. Indeed the relation $\ddot{x}_n + \eta \dot{x}_n = 0$ always holds, while the memory is not known *a priori*. As a consequence, we have to consider as independent initial conditions position, velocity, and memory. However, it is worth remarking that the comparison between the Lorenz system and the piecewise linearized one is completely meaningful. This because for the latter model w_{n-1} is easily known in terms of $\dot{\xi}_{n-1}$ and $\ddot{\xi}_{n-1}$ from Eq. (16): for the linearized system the choice of $\ddot{\xi}_{n-1}$ or of w_{n-1} is absolutely equivalent.

Since we are interested in the behavior of the Lorenz system in the chaotic steady state, all the following results are thus obtained via the numerical integration of the steady-state differential system

$$\begin{cases} \dot{x} = v \\ \dot{v} + \eta v + (x^2 - 1)x = -\alpha w x \\ \dot{w} = -\beta w + \beta(x^2 - 1), \end{cases} \quad (35)$$

where now $w = [x^2 - 1]_\beta$. This dynamical system, as already proved, is equivalent to the system (2) far from the initial transient.

We can now turn to the comparison with the piecewise linearized system. For the original Lorenz model we have computed the maps that relate τ_n and $|\dot{x}_n|$ to $|\dot{x}_{n-1}|$, respectively, by numerical integration of the system (35) (the notations are the same as in the previous section). Figures 19 and 20 show the results we obtained: the qualitative behavior of these maps is very similar to that of the analogous maps for the piecewise linearized system. As we will see, the mechanism for chaos to arise is indeed the same. Observe that the maps in Figs. 19 and 20 are not perfectly onto: obviously this is due to the fact that, in general, the Lorenz system does not reduce exactly to an one-dimensional map when the plane $x = 0$ is crossed.

From direct computation it appears that the residence time around a fixed point depends on the initial conditions in a way similar to that of the linearized system (Fig. 21). There is

a region in which τ_1 varies continuously with varying initial conditions and a region (Figs. 21 and 22) of strong instability. In the latter region τ_1 changes continuously along each “annulus” of the “spiral,” whereas it shows abrupt discontinuities crossing the boundary of each annulus. As expected, the system is attracted on that region (Fig. 23) and the maps in Figs. 19 and 20 derive from the overplotting between Figs. 23 and 22.

The chaos actually emerges due to the combination of the step-like first-exit-time (Fig. 19) and of the piecewise return map (Fig. 20) for initial conditions. This mechanism is the same as for the linearized model, for which we gave an analytical description. The results we obtained for the piecewise linearized system therefore provide in our opinion a useful enlightening tool to understand both the original Lorenz system and its eventual generalizations.

Finally, in order to point out the connection between the original Lorenz system and its piecewise linearized version, it is illuminating to compare the tent-like map shown by Lorenz in his original work [1] with the analogous map for our simplified system. Describing the relation between two consecutive maxima of the coordinate $z(t)$, Lorenz found a univocal tent-like map (Fig. 24). For our linearized system we obtain similar results (see Fig. 25). The growing branch of the map is approximately linear, since for small values of z the system evolution is confined in a half-space and, there, it essentially consists of an exponentially amplified oscillation. For large values of z the map has the same shape of the Lorenz tent-like map. The linear growing of the left branch of the map is due to the simplification we made on the evolution on each side of $x = 0$. The shape of the right branch shows that the piecewise linear system keeps all the complexity of the Lorenz model, which can be attributed to the unpredictability of the $x = 0$ crossing, which is the very origin of chaos in Lorenz-like systems.

VI. CONCLUSIONS

The main conclusions from the present paper can be summarized as follows. We have reformulated in a classical mechanics form the dynamics of Lorenz-like systems and showed that its three-dimensional phase-space dynamics can be mapped into an one-dimensional motion of a particle oscillating in a conservative quartic two-well potential, subjected to a viscous dissipation and to a memory forcing. Starting from this interpretation, we have introduced a piecewise linearized version of the Lorenz system (belonging to a larger family of Lorenz-like systems) which substantially has the same properties of the original model with the advantage that it allows an analytical treatment.

The most evident aspect of chaotic regime is the unpredictability of the instant at which the center of the particle amplified oscillation changes. Chaos arises due to the combination of the step-like behavior of this time with the piecewise return map defining the crossing conditions. This aspect has been singled out analytically, focusing on the piecewise linearized version. There, the exact equation for the time, at which the oscillation center changes, has been derived and the discontinuous dependence of this time on the crossing conditions has been shown analytically.

By means of numerical simulations we have verified that the highlighted mechanisms for the chaos to emerge survive also for the fully-nonlinear Lorenz system, where analytical techniques are not applicable.

ACKNOWLEDGMENTS

We would like to thank M. La Camera and A. Vulpiani for useful discussions and suggestions. This work was partially supported by the INFM project GEPAIGG01. D. V. was partially supported by the doctoral grants of the University of Nice and by grants of the University of Genova.

APPENDIX A: PARAMETERS α, β, η

In the Lorenz system, the following conditions for σ, b, r have to be satisfied in order to have three instable fixed points:

$$\sigma, b, r \in \mathbb{R}^+, \tag{A1a}$$

$$r > 1, \tag{A1b}$$

$$\sigma > b + 1, \tag{A1c}$$

$$r > r_c. \tag{A1d}$$

The parameters α, β, η are defined as follows:

$$\alpha = \frac{2\sigma}{b} - 1, \quad \beta = \sqrt{\frac{2b}{r-1}}, \quad \eta = \frac{\sigma + 1}{\sqrt{(r-1)b/2}}.$$

From (A1a) and (A1b) it immediately follows that α, β, η are positive too. Therefore, σ, b, r can be rewritten in terms of α, β, η in the form

$$\begin{aligned} \sigma &= -\frac{(1+\alpha)\beta}{\beta(\alpha+1) - 2\eta}, \\ r &= 1 - \frac{4}{\beta(\beta(\alpha+1) - 2\eta)}, \\ b &= -\frac{2\beta}{\beta(\alpha+1) - 2\eta}. \end{aligned}$$

Under the hypothesis $\alpha, \beta, \eta \in \mathbb{R}^+$, (A1a) and (A1b) are equivalent to

$$\beta(\alpha + 1) < 2\eta, \tag{A2}$$

while (A1c) corresponds to the inequality

$$\beta(\alpha + 1) > \beta + \eta. \tag{A3}$$

Specifically, (A1a), (A1b), and (A1c) then imply

$$\alpha > \frac{\eta}{\beta} > 1. \tag{A4}$$

Finally, (A1d) can be rewritten in terms of new parameters as

$$\alpha > \frac{\eta(2 + \beta(\beta + \eta))}{2\beta}, \quad (\text{A5})$$

from which necessarily (A4) follows.

APPENDIX B: FAMILY \mathcal{S}

The family of straight lines \mathcal{S} is defined by the equation

$$\mathcal{S}: \quad A(\tau_1) \dot{\xi}_0 + B(\tau_1) \ddot{\xi}_0 + C(\tau_1) = 0$$

where

$$A(\tau_1) = -2 \lambda_i \lambda_r e^{-\lambda_0 \tau_1} + e^{\lambda_r \tau_1} (2 \lambda_i \lambda_r \cos(\lambda_i \tau_1) + (\lambda_0^2 + \lambda_i^2 - \lambda_r^2) \sin(\lambda_i \tau_1))$$

$$B(\tau_1) = \lambda_i e^{-\lambda_0 \tau_1} + e^{\lambda_r \tau_1} ((\lambda_r + \lambda_0) \sin(\lambda_i \tau_1) - \lambda_i \cos(\lambda_i \tau_1))$$

$$C(\tau_1) = -\lambda_i (\lambda_i^2 + \lambda_r^2) e^{-\lambda_0 \tau_1} - \lambda_0 e^{\lambda_r \tau_1} [\lambda_i (2 \lambda_r + \lambda_0) \cos(\lambda_i \tau_1) + (\lambda_i^2 - (\lambda_0 + \lambda_r) \lambda_r) \sin(\lambda_i \tau_1)] + (\lambda_i (\lambda_i^2 + (\lambda_0 + \lambda_r)^2)).$$

1. Slope of straight lines of \mathcal{S}

We indicate with $(T_i)_{i \geq 0}$ the ordered sequence of the zeros of B : $T_i < T_{i+1} \forall i \geq 0$ with $B(T_i) = 0 \forall i \geq 0$. The first derivative of $-A/B$ is positive over the whole domain of definition. Indeed one has

$$-\frac{d}{d\tau_1} \left(\frac{A}{B} \right) =$$

$$\frac{\lambda_i e^{\lambda_r \tau_1} [\lambda_i e^{\lambda_r \tau_1} + e^{-\lambda_0 \tau_1} (-\lambda_i \cos(\lambda_i \tau_1) - (\lambda_0 + \lambda_r) \sin(\lambda_i \tau_1))] (\lambda_i^2 + (\lambda_0 + \lambda_r)^2)}{\lambda_i e^{-\lambda_0 \tau_1} + e^{\lambda_r \tau_1} [-\lambda_i \cos(\lambda_i \tau_1) - (\lambda_r + \lambda_0) \sin(\lambda_i \tau_1)]^2}$$

with

$$\lambda_i e^{\lambda_r \tau_1} + e^{-\lambda_0 \tau_1} (-\lambda_i \cos(\lambda_i \tau_1) - (\lambda_0 + \lambda_r) \sin(\lambda_i \tau_1)) > 0 \quad \forall \tau_1 \in \bigcup_{i=0}^{\infty} (T_i, T_{i+1}) \subset \mathbb{R}^+.$$

The latter inequality can be easily proved. Indeed:

$$\begin{aligned} (\lambda_r + \lambda_0) \tau_1 > \log(1 + (\lambda_r + \lambda_0) \tau_1) &\Rightarrow \\ e^{(\lambda_r + \lambda_0) \tau_1} > 1 + (\lambda_r + \lambda_0) \tau_1 > \cos(\lambda_i \tau_1) + \frac{(\lambda_r + \lambda_0)}{\lambda_i} \tau_1 &\Rightarrow \\ \lambda_i e^{\lambda_r \tau_1} > e^{-\lambda_0 \tau_1} (\lambda_i \cos(\lambda_i \tau_1) + (\lambda_r + \lambda_0) \sin(\lambda_i \tau_1)) &\quad \forall \tau_1 \in \bigcup_{i=0}^{\infty} (T_i, T_{i+1}) \subset \mathbb{R}^+. \end{aligned}$$

2. Envelope of family \mathcal{S}

A parametrical (not regular) representation of the envelope of the family \mathcal{S} is obtained deriving $\dot{\xi}_0$ and $\ddot{\xi}_0$ with respect to τ_1 . This can be done from the system

$$\begin{cases} A(\tau_1) \dot{\xi}_0 + B(\tau_1) \ddot{\xi}_0 + C(\tau_1) = 0 \\ \partial_{\tau_1} A(\tau_1) \dot{\xi}_0 + \partial_{\tau_1} B(\tau_1) \ddot{\xi}_0 + \partial_{\tau_1} C(\tau_1) = 0. \end{cases}$$

The result

$$\gamma : \begin{cases} \dot{\xi}_0 = \dot{\xi}_0(\tau_1) \\ \ddot{\xi}_0 = \ddot{\xi}_0(\tau_1) \end{cases}$$

is given by

$$\begin{aligned} \dot{\xi}_0(\tau_1) = & \frac{\{ -\lambda_0(\lambda_i(1 + e^{-\lambda_0\tau_1}) \cos(\lambda_i\tau_1) - \lambda_i(e^{-(\lambda_0+\lambda_r)\tau_1} + e^{\lambda_r\tau_1})) \\ & - (\lambda_r^2 + \lambda_i^2 - \lambda_0\lambda_r)(e^{-\lambda_0\tau_1} - 1) \sin(\lambda_i\tau_1) \}}{(\lambda_i e^{\lambda_r\tau_1} + e^{-\lambda_0\tau_1}(-(\lambda_0 + \lambda_r) \sin(\lambda_i\tau_1) - \lambda_i \cos(\lambda_i\tau_1)))} \end{aligned}$$

and

$$\begin{aligned} \ddot{\xi}_0(\tau_1) = & \frac{\{ \lambda_0^2(\lambda_i(\cos(\lambda_i\tau_1) - e^{\lambda_r\tau_1}) + \lambda_r \sin(\lambda_i\tau_1)) \\ & + (e^{-\lambda_0\tau_1} - 1)(\lambda_i \cos(\lambda_i\tau_1) - \lambda_r \sin(\lambda_i\tau_1))(\lambda_r^2 + \lambda_i^2) + \\ & - \lambda_0(e^{-\lambda_0\tau_1}((\lambda_i^2 - \lambda_r^2) \sin(\lambda_i\tau) + 2\lambda_i\lambda_r \cos(\lambda_i\tau_1)) - 2\lambda_i\lambda_r e^{-(\lambda_0+\lambda_r)\tau_1}) \}}{(\lambda_i e^{\lambda_r\tau_1} + e^{-\lambda_0\tau_1}(-(\lambda_0 + \lambda_r) \sin(\lambda_i\tau_1) - \lambda_i \cos(\lambda_i\tau_1))).} \end{aligned}$$

REFERENCES

- [1] E. N. Lorenz, *J. Atmos. Sci.* **20**, 130 (1963).
- [2] Lord Rayleigh, *Phil. Mag.* **32**, 529 (1916).
- [3] B. Saltzman, *J. Atmos. Sci.* **19**, 329 (1962)
- [4] K. Pyragas, *Phys. Rev. Lett.* **86**, 2265 (2001).
- [5] D. Xu, *Phys. Rev. E.* **63**, 027201 (2001).
- [6] H. Nijmeijer, *Physica D* **154**, 219 (2001).
- [7] S. Iplikci and Y. Denizhan, *Physica D* **150**, 163 (2001).
- [8] M. Clerc, P. Couillet, and E. Tirapegui, *Phys. Rev. Lett.* **83**, 3820 (1999).
- [9] C. Raab and J. Kurths, *Phys. Rev. E* **64**, 016216 (2001).
- [10] D. Pingel and P. Schmelcher, *Phys. Rev. E* **64**, 026214 (2001).
- [11] G. Yan and L. Yuan, *Physica D* **154**, 43 (2001).
- [12] J.B. Gao, *Phys. Rev. E* **63**, 066202 (2001).
- [13] C.P. Unsworth, M.R. Cowper, S. McLaughlin, and B Mulgrew, *Physica D* **155**, 51 (2001).
- [14] A. d’Anjou, C. Sarasola, F.J. Torrealdea, R. Orduna, and M. Graña, *Phys. Rev. E.* **63**, 046213 (2001).
- [15] D. Pazó, N. Montejo, and V. Pérez-Muñuzuri, *Phys. Rev. E.* **63**, 066206 (2001).
- [16] H. Busch, M.-Th. Hütt, and F. Kaiser, *Phys. Rev. E* **64**, 021105 (2001).
- [17] W. Tucker, *C. R. Acad. Sci.* **328**, 1197 (1999).
- [18] I. Stewart, *Nature* **406**, 948 (2000).
- [19] R. Festa, A. Mazzino, and D. Vincenzi, *Europhys. Lett.* (to be published).
- [20] C. Sparrow, *The Lorenz Equations: Bifurcations, Chaos, and Strange attractors* (Springer Verlag, New York, 1982) vol. 41 of Applied Mathematical Sciences.
- [21] F.C. Moon and P.J. Holmes, *J. Sound Vib.* **65**, 285 (1979); **69**, 339 (1980).
- [22] Eq. (18) describes a single loop feedback system (in the absence of input) with linear transfer function $[s^3 + (\beta + \eta)s^2 + (1 + \beta\eta)s + \beta(1 + \alpha)]^{-1}$ and nonlinear feedback $-\beta(1 + \alpha)\text{sgn}(x)$.
- [23] A.A. Andronov, A.A. Vitt, and S. E. Khaiken, *Theory of oscillators* (Pergamon, Oxford, 1966).
- [24] C.T. Sparrow, *J. Math. An. Appl.* **83**, 275 (1981).
- [25] S.W. Shaw and P.J. Holmes, *J. Sound Vib.* **90**, 129 (1983).
- [26] T. Matsumoto, L.O. Chua, and M. Komuro, *Physica D* **24**, 97 (1987).
- [27] T. Yang and L.O. Chua, *Int. J. Bifurcations Chaos* **10**, 2015 (2000).
- [28] The continuity at $x = 0$ of \dot{x} and $[|x|]_\beta$ corresponds to the continuity of x , $y = x + \dot{x}/\sigma$ and $z = (b/2\sigma)|x| + (1 - b/2\sigma)[|x|]_b$.
- [29] P. Lancaster, *Theory of Matrices with applications* (Academic Press, Orlando Florida, 1985)
- [30] J. Guckenheimer and P. Holmes, *Nonlinear Oscillations, Dynamical Systems, and Bifurcations of Vector Fields*, (Springer Verlag, New York, 1983).
- [31] For the sake of simplicity we frequently speak of “initial conditions” for a trajectory after a generic collision. Obviously, we refer to the conditions that a solution, which matches to a preceding trajectory, must satisfy in $x = 0$. We always consider the evolution of the system in the steady-state and so far from the initial transient.

FIGURES

FIG. 1. The constant-in-time quartic potential U ($\sigma = 10$, $b = 8/3$, $r = 28$). The classical particle representing the Lorenz system moves in the potential U subjected to a viscous damping and to a memory forcing. The minima of the potential wells correspond to the unstable points of the three-dimensional Lorenz system.

FIG. 2. Typical chaotic phase portrait for the original Lorenz model ($\eta = 1.31$, $\alpha = 10.30$, $\beta = 0.216$).

FIG. 3. Typical chaotic phase portrait for the inverse parametrically forced Duffing equation ($\eta = 1.31$, $A = 4.2$, $\Omega = 0.99$). The chaotic evolution of this system is characterized by the competition between a viscous friction and a forcing term with the same structure of the right hand side of the Lorenz equation. Here, however, the forcing is externally given and the memory is replaced by a known function of time.

FIG. 4. Quartic potential U for the original Lorenz system (dashed line) and for the piecewise linearized system (full line). The linearization of the Lorenz system maintains the qualitative shape of the constant-in-time potential.

FIG. 5. Typical chaotic phase portrait for the original Lorenz system ($\sigma = 10$, $b = 8/3$, $r = 28$).

FIG. 6. Typical chaotic phase portrait for the piecewise linearized Lorenz system ($\sigma = 10$, $b = 8/3$, $r = 55$).

FIG. 7. Stable and unstable manifolds for the point $\boldsymbol{\xi} = \mathbf{0}$ in the phases space ξ , $\dot{\xi}$, $\ddot{\xi}$. The evolution of the piecewise linearized system on each side of π consists of an exponential decay along \mathcal{W}^s and of an amplified oscillations on \mathcal{W}^u .

FIG. 8. Graphical interpretation of the discontinuous character of τ_1 for small changes of the initial condition. Full line is the curve $g(\tau_1)$, dashed lines is $h(\tau_1)$ for the parameters $\alpha = 6.50$, $\beta = 0.19$, $\eta = 0.78$. Bullets denotes the first intersection between g and h , whose abscissa defines the residence time.

FIG. 9. Slope of the straight lines of the family \mathcal{S} ($\alpha = 6.50$, $\beta = 0.19$, $\eta = 0.78$). [See Eq. (26) and Appendix B for the exact definition.]

FIG. 10. Ordinate for $\dot{\xi}_0 = 0$ of the straight lines of the family \mathcal{S} ($\alpha = 6.50$, $\beta = 0.19$, $\eta = 0.78$). [See Eq. (26) and Appendix B for the exact definition.]

FIG. 11. The family of curves \mathcal{S} [defined in Eq. (26)] for $\alpha = 6.50$, $\beta = 0.19$, and $\eta = 0.78$.

FIG. 12. The envelope γ of the family of straight lines \mathcal{S} looks similar to a spiral ($\alpha = 6.50$, $\beta = 0.19$, and $\eta = 0.78$).

FIG. 13. Contour lines of the residence time τ_1 as a function of the initial conditions $(\dot{\xi}_0, \ddot{\xi}_0)$ for $\tau_1 \in [0, T_2]$ ($\alpha = 6.50$, $\beta = 0.19$, $\eta = 0.78$).

FIG. 14. Graph of τ_1 as a function of the initial conditions, obtained by numerical solution of the transcendental equation (25) ($\alpha = 6.50$, $\beta = 0.19$, $\eta = 0.78$).

FIG. 15. Map of the first-exit time τ_n as a function of the crossing velocity $\dot{\xi}_n$, obtained by numerical solutions of Eqs. (27) and (30). ($\alpha = 6.50$, $\beta = 0.19$, $\eta = 0.78$)

FIG. 16. During chaotic evolution the couple of crossing conditions $(\dot{\xi}_n, \ddot{\xi}_n)$ is attracted on the straight line \mathcal{L}^+ , which is superimposed to the instability region of the residence time τ_n (identified by the curve γ). The graph refers to the values $\alpha = 6.50$, $\beta = 0.19$, $\eta = 0.78$.

FIG. 17. The velocity $\dot{\xi}_n$ at the n -th crossing of the plane $x = 0$ as a function of the velocity $\dot{\xi}_{n-1}$ ($\alpha = 6.50$, $\beta = 0.19$, $\eta = 0.78$). Notice that, however, in the steady-state chaotic evolution the map is restricted to the range $(0, 1.2)$ of possible values of $\dot{\xi}_{n-1}$.

FIG. 18. Attraction of the piecewise linearized system on the manifolds \mathcal{W}_\pm^u . The evolution of the system on each side of π consists of a “rapid” exponential decay along the stable manifold and of a “slow ” amplified oscillation on the unstable manifold.

FIG. 19. Map $\tau_n = \tau_n(|\dot{x}_{n-1}|)$ for the original Lorenz system, obtained by numerical integration of the system (35) ($\alpha = 10.30$, $\beta = 0.216$, $\eta = 1.31$).

FIG. 20. Map between $|\dot{x}_n|$ and $|\dot{x}_{n-1}|$ for the original Lorenz system, obtained by numerical integration of the system (35) ($\alpha = 10.30$, $\beta = 0.216$, $\eta = 1.31$).

FIG. 21. Graph of τ_1 as a function of the crossing conditions for the original Lorenz system, obtained by numerical integration of the system (35) for different initial conditions ($\alpha = 10.30$, $\beta = 0.216$, $\eta = 1.31$),

FIG. 22. Graph of τ_1 as a function of the crossing conditions viewed from the above in the case of the original Lorenz system ($\alpha = 10.30$, $\beta = 0.216$, $\eta = 1.31$).

FIG. 23. Map between the crossing memory w_n and the corresponding crossing velocity $|\dot{x}_n|$ for the original Lorenz system ($\alpha = 10.30$, $\beta = 0.216$, $\eta = 1.31$).

FIG. 24. The tent-like map for the original Lorenz system ($b = 8/3$, $\sigma = 10$, $r = 28$). M_n denotes the n -th maximum of the coordinate $z(t)$.

FIG. 25. The tent-like map for the piecewise linearized system ($b = 8/3$, $\sigma = 10$, $r = 100$).

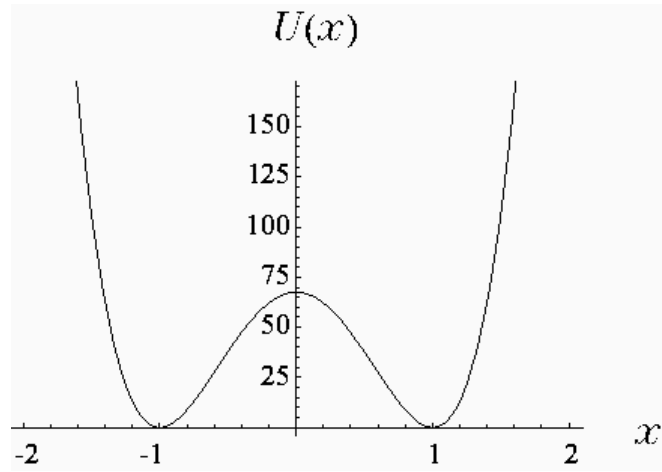


FIG. 1. R. Festa *et al.*, Phys. Rev. E

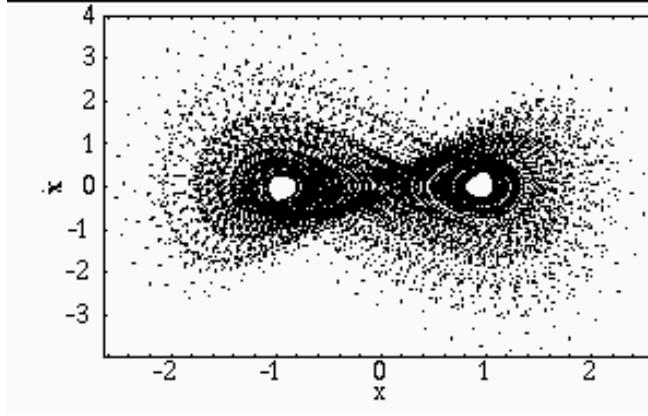


FIG. 2. R. Festa *et al.*, Phys. Rev. E

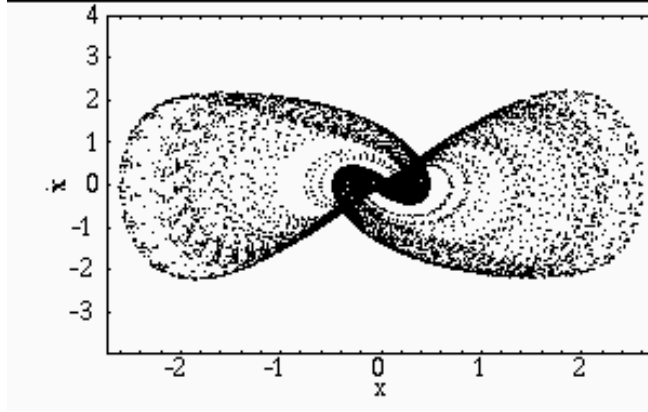


FIG. 3. R. Festa *et al.*, Phys. Rev. E

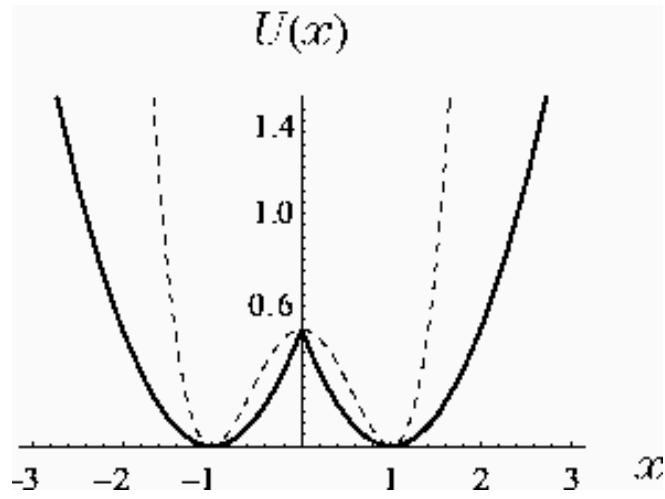


FIG. 4. R. Festa *et al.*, Phys. Rev. E

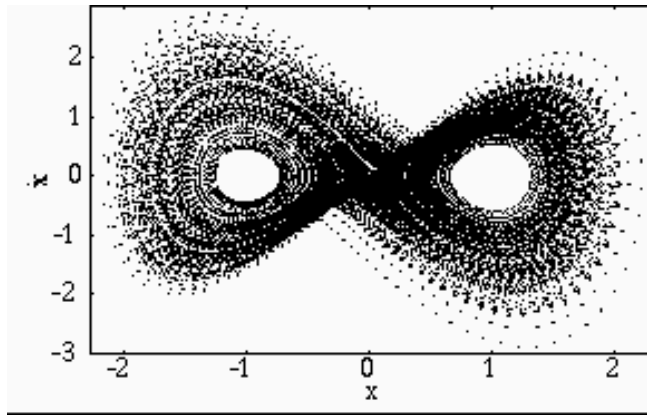


FIG. 5. R. Festa *et al.*, Phys. Rev. E

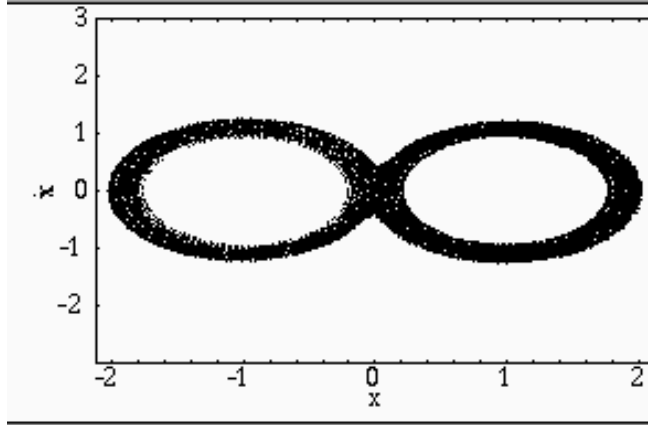


FIG. 6. R. Festa *et al.*, Phys. Rev. E

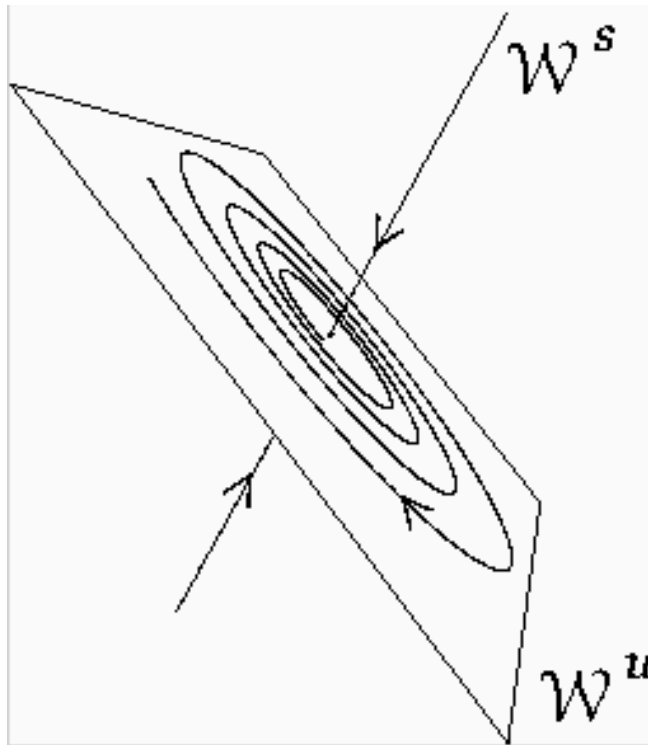


FIG. 7. R. Festa *et al.*, Phys. Rev. E

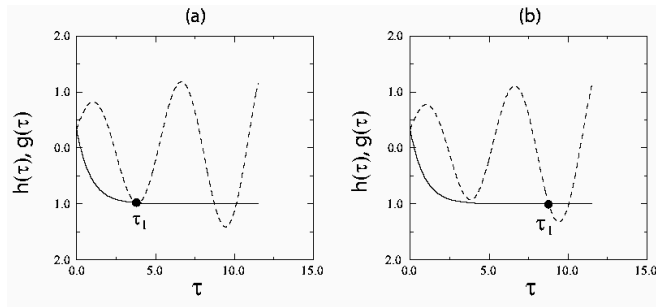


FIG. 8. R. Festa *et al.*, Phys. Rev. E

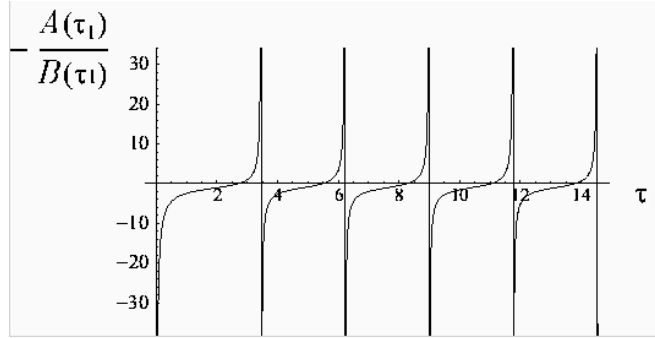


FIG. 9. R. Festa *et al.*, Phys. Rev. E

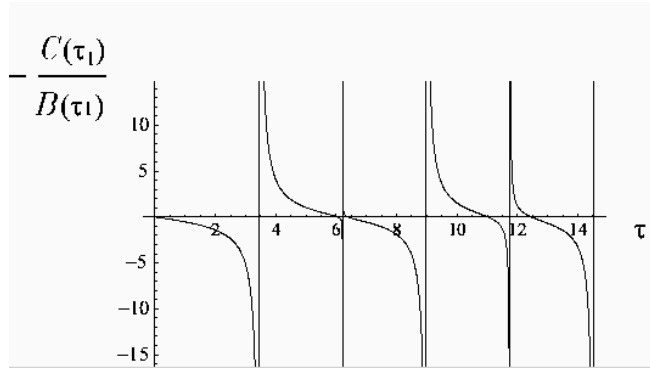


FIG. 10. R. Festa *et al.*, Phys. Rev. E

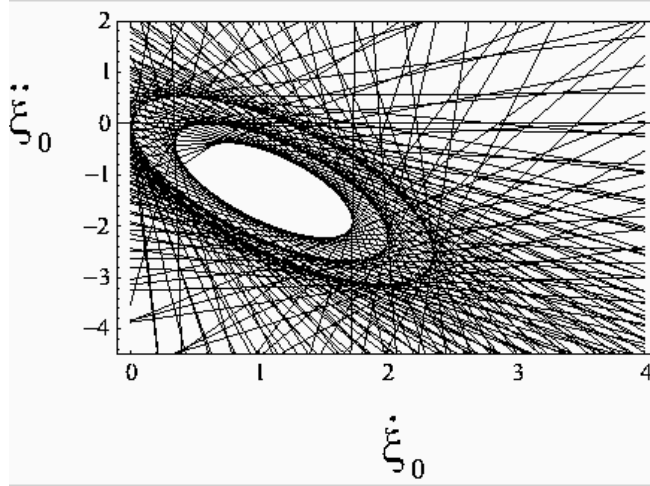


FIG. 11. R. Festa *et al.*, Phys. Rev. E

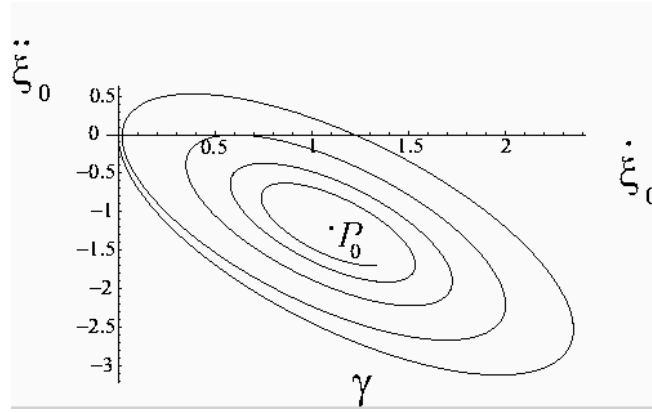


FIG. 12. R. Festa *et al.*, Phys. Rev. E

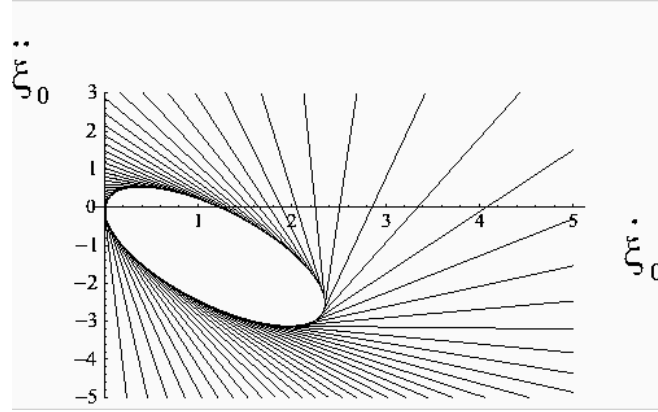


FIG. 13. R. Festa *et al.*, Phys. Rev. E

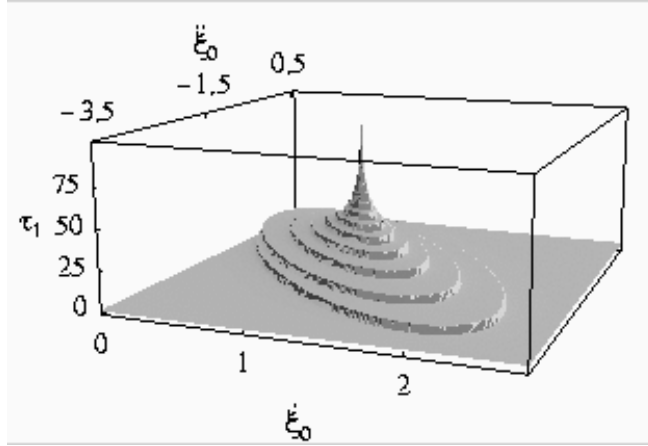


FIG. 14. R. Festa *et al.*, Phys. Rev. E

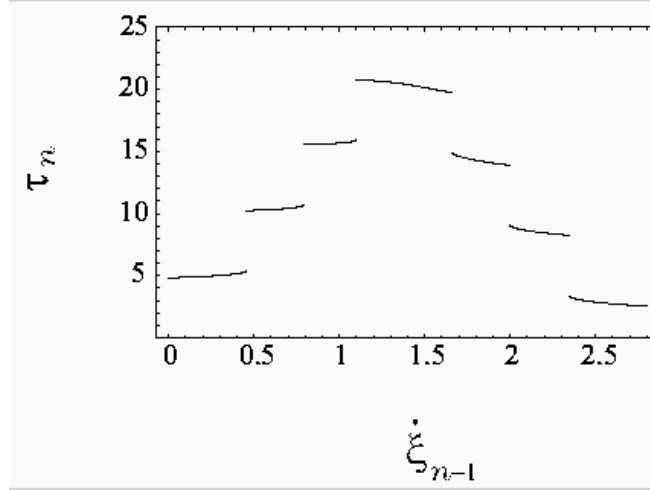


FIG. 15. R. Festa *et al.*, Phys. Rev. E

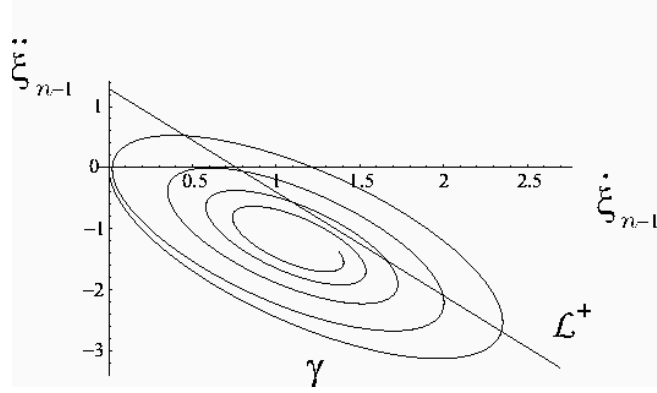


FIG. 16. R. Festa *et al.*, Phys. Rev. E

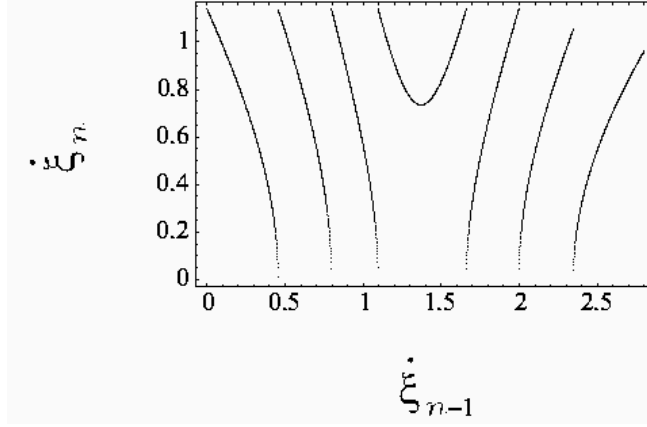


FIG. 17. R. Festa *et al.*, Phys. Rev. E

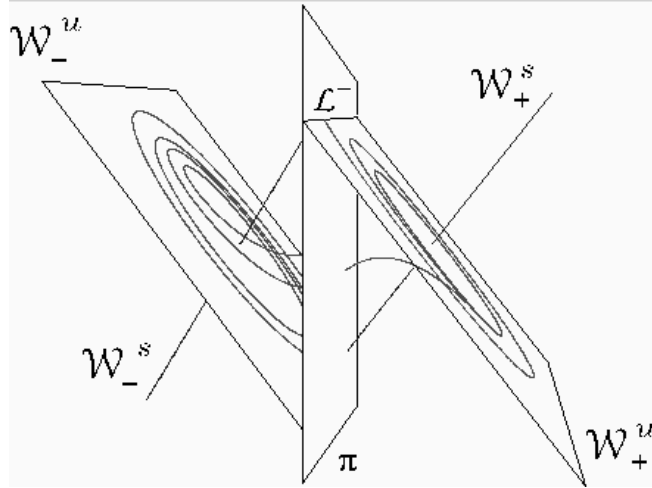


FIG. 18. R. Festa *et al.*, Phys. Rev. E

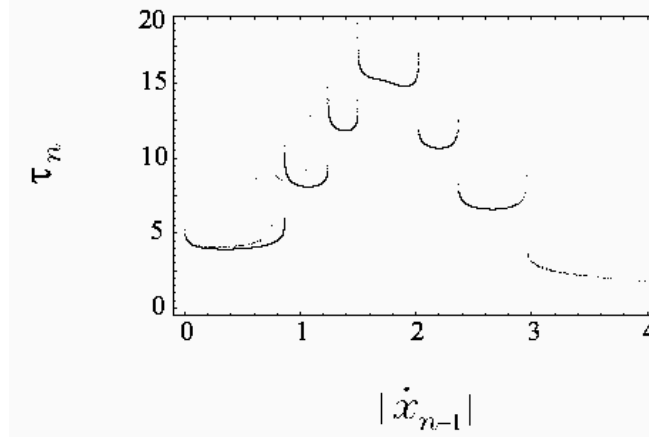


FIG. 19. R. Festa *et al.*, Phys. Rev. E

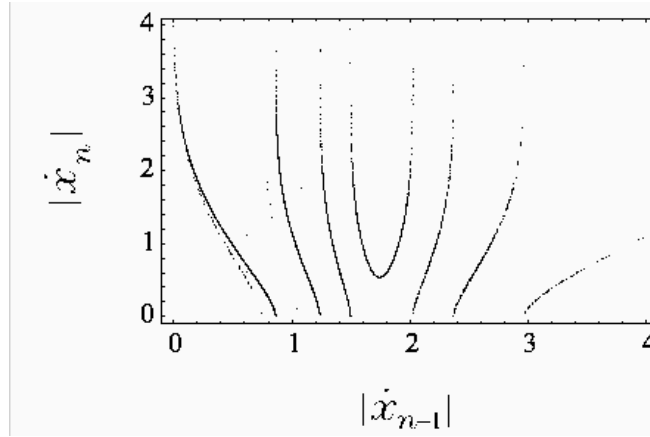


FIG. 20. R. Festa *et al.*, Phys. Rev. E

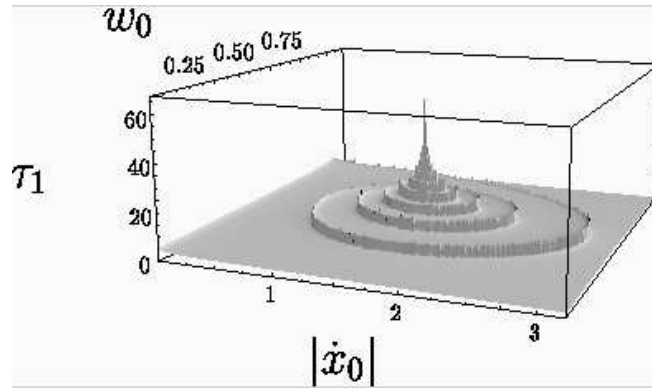


FIG. 21. R. Festa *et al.*, Phys. Rev. E

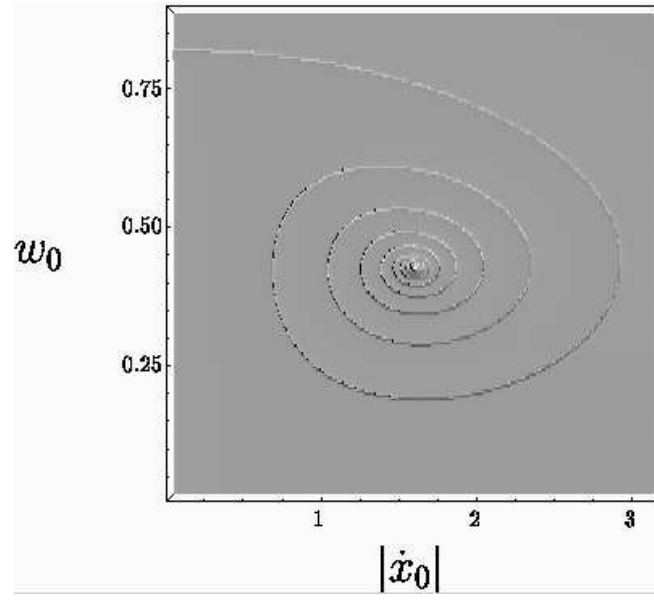


FIG. 22. R. Festa *et al.*, Phys. Rev. E

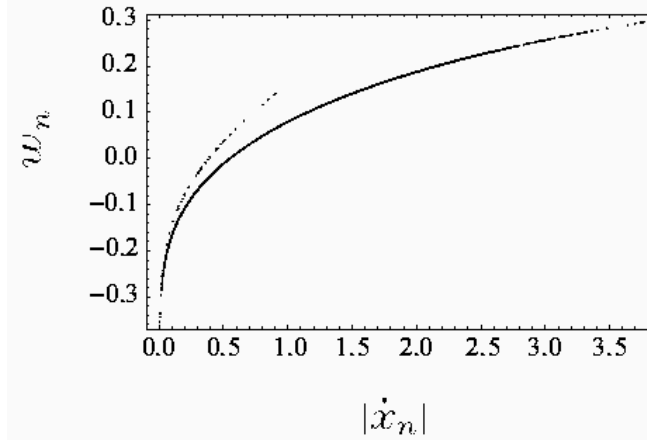


FIG. 23. R. Festa *et al.*, Phys. Rev. E

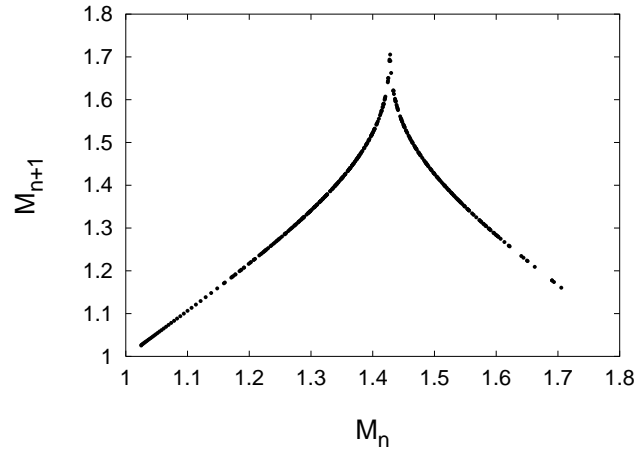


FIG. 24. R. Festa *et al.*, Phys. Rev. E

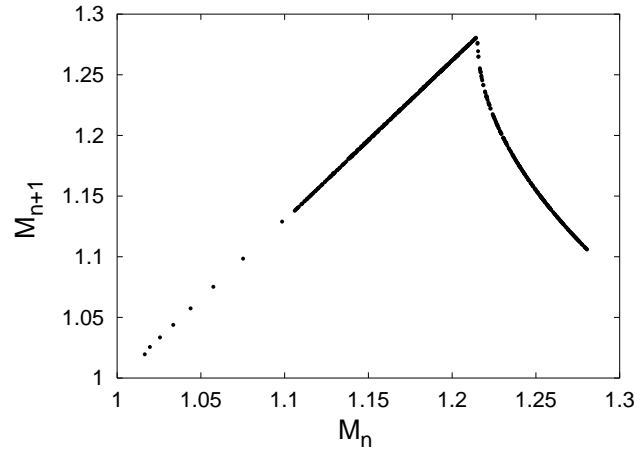


FIG. 25. R. Festa *et al.*, Phys. Rev. E